IEICE TRANS. COMMUN., VOL.E107–B, NO.10 OCTOBER 2024

PAPER

Global Navigation Satellite System Signal Phase Combining and Performance of Distributed Antenna Arrays

Wenfei GUO[†,††], **Jun ZHANG**[†], **Chi GUO**[†a)], ***and*** **Weijun FENG**[†], ***Nonmembers***

SUMMARY Low signal power and susceptibility to interference cause difficulties for traditional global navigation satellite system (GNSS) receivers in tracking weak signals. Extending coherent integration time is a common approach for enhancing signal gain. However, coherent integration time cannot be indefinitely increased owing to navigation bit sign transition, receiver dynamics, and clock noises. This study proposes a cross-correlation phase combining (CPC) algorithm suitable for distributed multi-antenna receivers to improve carrier-tracking performance in weak GNSS signal conditions. This algorithm cross-correlates each antenna's intermediate frequency (IF) signal and local carrier to detect the phase differences. Subsequently, the IF signals are weighted to achieve phase alignment and coherently combined. The carrier-to-noise ratio (CNR) and carrier phase equation of the combined signal were derived for the CPC algorithm. Global positioning system (GPS) signals received by distributed antenna array with six elements were used to validate the performance of the algorithm. The results demonstrated that the CPC algorithm could effectively achieve signal phase alignment at 32 dB-Hz, resulting in a combined-signal CNR enhancement of 6 dB. The phase-tracking error variance was reduced by 72% at 30 dB-Hz compared with that of a single-antenna signal. The algorithm exhibited low phased array calibration requirements, overcoming the limitations associated with coherent integration time and effectively enhancing tracking performance in weak-signal environments.

key words: *weak GNSS signal, coherent integration, distributed antenna arrays, multi-antenna signal combining*

1. Introduction

Global navigation satellite system (GNSS) provides users with positioning, navigation, and timing functions. GNSS has steadily developed over the past decades, and satellite navigation receiver applications have increased across various fields [1]. However, the satellite navigation signal power reaching the Earth's surface is weak owing to high free-space loss and attenuation while traveling through the atmosphere and ionosphere. Even in open outdoor environments, the signal strength is only approximately −130 dBm [2]. Receivers exhibit a decline in signal power in harsh environments. For example, trees in forests and buildings in urban areas obstruct signals and weaken signal strength. In addition, these signals may be subjected to cross-correlation interference from powerful satellites or interfering signals [3] and multipath interference [4]. In such environments, the received signal-to-noise ratio (SNR) can be attenuated by 10–30 dB [5], resulting in severe signal deterioration.

The low signal power in weak-signal environments causes the SNR of the signal input to the tracking loop phase discriminator to be extremely low, leading to considerable errors in the output of the carrier-tracking loop or even a loss of lock. Conventional carrier-tracking loops cannot adapt to weak-signal environments. Local and international researchers have extensively studied high-sensitivity carrier-tracking technologies, including loop optimization, coherent integration extension, external assistance, vector-tracking loop, and high-sensitivity tracking algorithms [6], [7]. Coherent integration extension is the most direct and commonly used method for enhancing SNR gain. However, this approach has various limitations, such as the bit sign transition of navigation data, receiver and satellite dynamics, and frequency stability of crystal oscillators [8]–[10]. For the commonly used global positioning system (GPS) L1 C/A signal, noncoherent integration can eliminate navigation data but introduces quadratic loss [1]. The acceleration caused by the receiver and satellite motions and the frequency drift of the crystal oscillator of the receiver limit the coherent integration gain. Scholars have proposed methods for estimating satellite dynamics based on satellite orbit approximation [11]. The receiver dynamics and frequency drift of the crystal oscillator are crucial for long-term coherent integration, significantly affecting the performance of the receiver [12].

Compared with single-antenna signals, combining antenna array signals provides numerous advantages, such as stable system performance, effective enhancement of signal reception quality, high antenna utilization, cost savings, and ease of maintenance [13]. The wireless channel is coherent for satellite navigation signals. This implies that the antenna array elements receiving the signal differ only in amplitude and phase when multipath effects are disregarded [14], [15]. Although the signal is distorted owing to the nonlinearity of the satellite devices, this distortion does not change the coherence of the wireless channel itself. Because the signals received by individual antenna array elements are correlated, and the noise remains mutually independent, the signals from different propagation channels can be constructively combined in the spatial domain. Adjusting the array signal phase weights and coherently adding these signals leads to signal gain, enhancing the SNR [16].

Array antenna systems are typically categorized as phased or distributed. Unlike their phased array counterparts, distributed array antennas do not have strict half-

Manuscript received November 28, 2023.
Manuscript revised February 23, 2024.
Manuscript publicized May 14, 2024.
[†]Wuhan University, Wuhan, 430072, China.
[††]Institute of Electronic Information, Wuhan Qingchuan University, Wuhan, 430204, China.
a) E-mail: guochi@whu.edu.cn
DOI: 10.23919/transcom.2023EBP3191

wavelength requirements for the position of the array elements. The gain of the signal combined in the distributed array antennas is unrelated to the arrival direction, but only to the received SNR and carrier phase. This phenomenon confers distributed arrays with heightened flexibility, maneuverability, and a high gain advantage [17]. Currently, the algorithms for signals combining distributed array antennas include SIMPLE [18], SUMPLE [19], EIGEN [20], and LSFIT [21]. Although the LSFIT algorithm boasts minimal combining loss, it requires cross-correlation functions among all antenna signals, resulting in the calculation amount being proportional to the square of the antenna count. By contrast, the SUMPLE algorithm requires a number of calculations proportional to the number of antennas. This value closely matches that of the SIMPLE algorithm; however, it delivers a performance comparable to that of the LSFIT algorithm. Therefore, the SUMPLE algorithm is widely used for combining multi-antenna signals.

Rogstad originally introduced the SUMPLE algorithm in 2005. Subsequently, he described the SUMPLE algorithm comprehensively and analyzed its performance from various aspects. Xu et al. conducted a comparative study between the SUMPLE and SIMPLE algorithms and found the SUMPLE algorithm superior to the SIMPLE algorithm [22]. Chen et al. used a minimum mean-squared error estimator to amplify the performance of the SUMPLE algorithm [23]. Wang et al. improved the combined performance of the SUMPLE algorithm by identifying and excluding low-quality signal paths by assessing gain factors [24]. Yan et al. applied the SUMPLE algorithm to large-scale antenna arrays on a CPU-GPU heterogeneous system without experimental verification or algorithm performance improvement [25]. Li et al. enhanced the SNR of the input signal by resampling and used the SUMPLE algorithm for signal combination but without any algorithm enhancements [26]. These studies have extensively analyzed and improved the SUMPLE algorithm from different perspectives and applied it to various domains; however, the application of the algorithm in GPS systems remains unexplored. Currently, the G-STAR developed by Lockheed Martin [27]and the Integrated GPS Anti-Interference System (IGAS) developed by Rockwell Collins [28] are both mature satellite navigation antenna array receivers. However, the digital signal combining technology that has been maturely applied in existing products is non-blind beamforming. Non-blind beamforming requires the use of external information sources such as inertial navigation systems (INS) to calibrate the position and elevation of the antenna array [29]. However, in normal scenarios, it is difficult to bear the cost of adding an inertial navigation system. Therefore, a signal-combining technology suitable for distributed arrays that does not require DOA information and reducing dependence on external information sources is an important development trend for GPS signal combing.

This study introduced a cross-correlation phase combining (CPC) algorithm to address the difficulty of GPS tracking in a weak-signal environment and overcome the challenges of existing methods, primarily single-antenna GPS systems. During the GPS signal tracking process, the phase-locked loop (PLL) generates a local carrier matching the signal carrier of the antenna. This local carrier is considered as a beneficial factor because it can be employed as a stable phase input to enhance the phase stability of the combined signal and can also serve as an independent signal input for phase-offset determination, enhancing accuracy. In this algorithm, one antenna signal of the array is selected in turn, and the weighted sum of the remaining antenna signals and local carrier are the reference signals. The selected antenna and reference signals are cross-correlated to calculate the phase offset between them, which is then used for phase compensation of the antenna signal. Owing to the inclusion of a fixed-phase component of the local carrier in the reference signal, the antenna signal phase converges toward the local carrier. In the next iteration, as the signal tends to be coherently added, the SNR of the reference signal increases, and the phase offset compensation value approaches the actual value. Consequently, after a sufficient number of iterations, the combined-signal phase gradually aligns with the local carrier phase.

This study analyzed the CNR and carrier phase of the signals using the CPC algorithm. GPS signals received by distributed antenna array with six elements were used to evaluate the performance of the algorithm. The remainder of this paper is structured as follows: Section 2 discusses the distributed antenna array signal model; Section 3 elaborates on the CPC algorithm and introduces the structure of the multi-antenna signal-combining system; Section 4 analyzes the CNR and carrier phase of the combined signals using the CPC algorithm, delineates the factors influencing the signal-combining performance, and presents the simulation experiment; Section 5 presents the simulation and performance analysis results; and Sect. 6 summarizes the conclusions.

2. Distributed Array Antenna Signal and System Model

Figure 1 shows the structure of the signal combination system. Consider L antennas in a distributed antenna system situated at diverse locations but working in the same frequency band. Generally, the distance between the distributed antenna array elements is greater than half the wavelength, and the antenna is freely distributed in three-dimensional (3D) space [30].

In practice, factors, such as various spatial positions of antennas in a distributed array and inconsistencies in the phase attributes of the radio frequency front-end (RFFE) and signal transmission channels, contribute to the phase offsets among signals received by different antennas. Therefore, before signal combination, a phase alignment should be performed to increase signal coherence. Phase alignment involves using multi-antenna signal correlation processing to estimate the phase offsets among distinct intermediate frequency (IF) signals and achieve signal carrier phase consistency through the phase rotation factor. The phase rotation

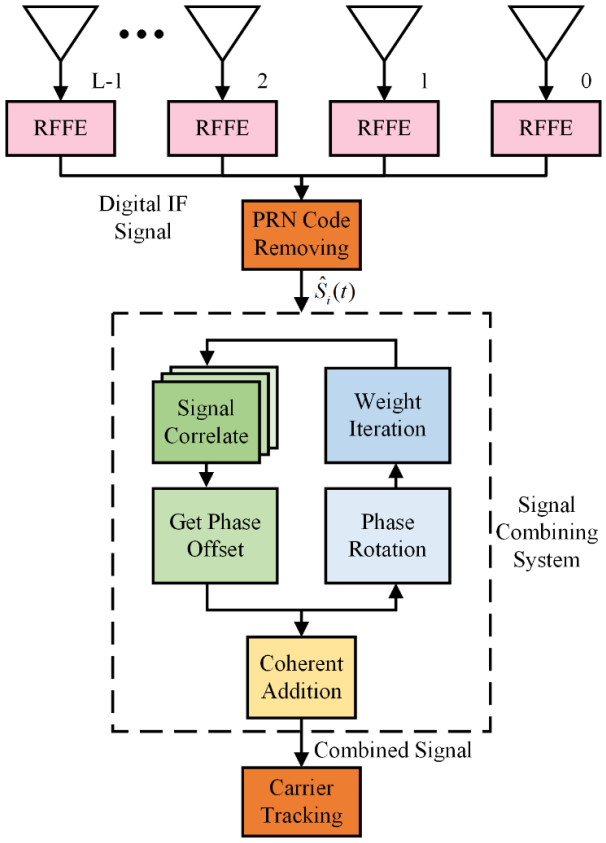

Fig. 1 Array antenna signal-combining system.

factor is defined as the phase weight and is iteratively updated continuously. Section 3 presents a detailed analysis. Upon successful phase alignment, the coherently combined signals are output to the PLL loop, and the combined signal is carrier-tracked.

The GPS signal received by the antenna includes signals from all satellites in the sky. Thus, when estimating the phase offset of a particular satellite signal through signal correlation, other satellite signals are considered as interference. This can seriously affect the accuracy of the phase-offset estimation. Therefore, in this study, the signal-combining system processed the pseudo-code-stripped IF signal. Pseudocode is stripped through native pseudocode. The local pseudocode, like the local carrier, is fed back from the subsequent tracking process. The IF signals addressed in this study only include navigation signals received by antenna from a single satellite signal.

After down conversion by the RFFE and the removal of the pseudo-random noise codes, the digital IF signal from antenna 0 can be expressed as follows:

$$S_0(t) = \alpha_0 D_0(t) sin\left(\omega_{IF} * t + \theta_0\right) + n_0(t), \tag{1}$$

where α_0 represents the amplitude coefficient of the received signal, $D_0(t)$ represents the data level containing the navigation information, ω_{IF} represents the carrier frequency after mixing under RFFE, θ_0 represents the carrier phase of the *0-th* antenna, $n_0(t)$ represents the noise component in the reference signal. Considering the phase offsets between the various antenna signals relative to the reference antenna, the received signals from the remaining $L-1$ antennas can be expressed as follows:

$$\begin{aligned} S_i(t) &= \alpha_i D_i(t) sin\left(\omega_{IF} * (t+\tau_i) + \theta_0\right) + n_i(t), \\ & i = 1, 2, \ldots, L-1, \end{aligned} \tag{2}$$

where the subscript i denotes the antenna number, and τ_i represents the time delay of the signal from the $L-1$ antennas relative to the reference antenna signal; the time delay τ_i encompasses differences in antenna circuitry, RFFE channel hardware delays, and transmission path delays due to varying antenna positions, leading to IF carrier phase offset. No correlation was assumed between the navigation signal and noise among the various antennas.

Complex signals are vital to signal-combining systems owing to the need for cross-correlation operations. By modifying Euler's formula, the received signal of the entire distributed antenna system can be defined as follows [31]:

$$\hat{S}_i(t) = \hat{s}_i(t) e^{j\omega_{IF}\tau_i} + \hat{n}_i(t), \tag{3}$$

where the hat symbol $\widehat{(\cdot)}$ above the signal and noise indicates that they are complex signals, and $\hat{s}_i(t) = \alpha_i D_i(t) e^{j[\omega_{IF} * t + \theta_0]}$ represents the signal component. Without signal tracking, prior information on the satellite signal incident angle, and uncertainty in amplitude and phase caused by antenna deployment and radio frequency channels, the phase offsets result in an inequality in the carrier phase among various antenna signals, resulting in a CNR loss [32], [33]. Therefore, obtaining phase offsets among various antenna signals and compensating for this difference to align the signals are crucial for signal phase combination.

3. Cross-Correlation Phase Combining Algorithm

Aligning the phase delays of signals is essential for coherently combining antenna signals in a distributed antenna array system. When estimating the phase offsets between signals in an antenna array, the relative phase offset can be estimated by correlating the signals. If the CNR of each antenna signal is sufficiently high, all antenna pairs can exhibit strong correlations, no special processing will be required, and the phase offsets derived from the correlation can be directly used to align the signal [13]. By contrast, when the CNR is low, other methods must be employed. For example, If the user is in an urban area, the geometric structure of the building, wall thickness, etc. can attenuate the signal by 10–25 dB, and the signal power attenuation caused by the indoor environment can reach 25–30 dB [34]. In weak signal environment, it is necessary to use all possible antenna pairs to improve the phase alignment performance, reducing the CNR loss caused by phase estimation errors.

Figure 2 shows the structure of the multi-antenna signal-combining system. The IF signal represents the IF digital signal that completes the pseudo-code stripping. The

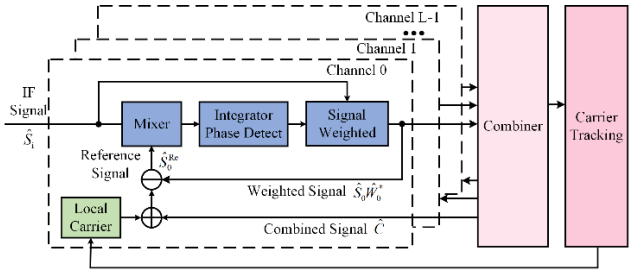

Fig. 2 Structure of the multi-antenna signal-combining system.

IF signal of each channel is cross-correlated with the reference signal, and the phase detector outputs the phase offset between the two, which is the phase weight. The IF signal is phase-compensated through the phase weight, and then the signals of all the antennas are input to the combiner and added. The reference signal is generated by adding the combined signal and local carrier and then subtracting the IF signal. The local carrier of each channel is consistent and fed back by the PLL. Following multiple iterations, the phase detector output gradually converges to zero, completing the phase alignment. After the phase alignment, a coherent combination enhances the combined-signal CNR. The calculation amount of the CPC algorithm is proportional to the number of array elements, requires L correlators, and is slightly more complex than the SUMPLE algorithm. Compared with the SUMPLE algorithm, the CPC algorithm requires L additional adders.

Figure 3 shows a flowchart of the CPC algorithm. For each antenna channel, the antenna signal is correlated with the reference signal to generate phase weights. Each L-antenna IF signal sequentially performs correlation and weighting operations, and the weighted IF signals are coherently combined to form an iteration. The phase weights $\hat{W}_i$ begin with a phase-zero unit vector. After each iteration, a new weight replaces the previous weight, and this process is repeated. The algorithm converges after several iterations. After achieving phase alignment for all antenna signals, they are coherently combined to produce the output.

In the CPC algorithm, the local carrier enhancing the CNR of the reference signal and improving algorithm performance. Simultaneously, during the signal phase alignment process, the phase center of the local carrier remains unchanged, no phase jitter occurs, and the local carrier participates in all reference signals, which is equivalent to introducing a fixed component into the reference signal. Throughout each iteration, the process gradually aligns the phase of each antenna signal toward this fixed component, ultimately converging to it. Thus, the CPC algorithm effectively estimates the phase offset and retains the advantages of the conventional algorithms.

From Eq. (3), the *i-th* antenna signal of the antenna array and weight phase in the correlation-weighting process can be expressed as follows:

$$\hat{S}_i(t) = \hat{s}_i(t) + \hat{n}_i^s(t), \tag{4}$$

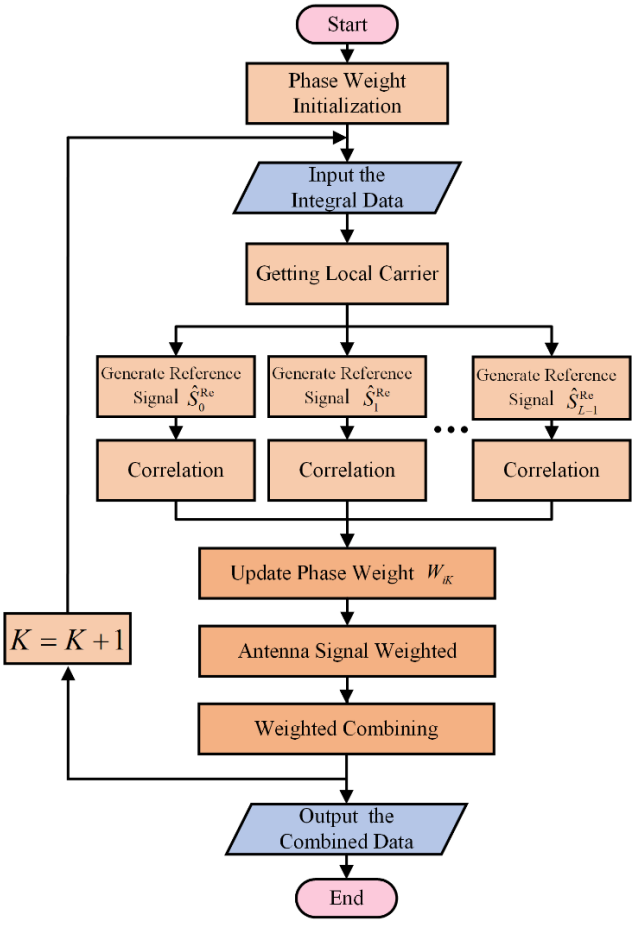

Fig. 3 Flowchart of the CPC algorithm.

$$\hat{W}_{iK} = \hat{w}_{iK} + \hat{n}_{iK}^w, \tag{5}$$

where $\hat{s}_i(t)$ and $\hat{n}_i^s$ represent the signal and noise components, respectively. $\hat{W}_{iK}$ represents the phase weight within an iteration. The number of correlated sampling points is the correlation averaging time, recorded as N, and the subscript K represents a time variable measured in the correlation time interval N units. Furthermore, $\hat{w}_{iK}$ represents the ideal weighting coefficient, and $\hat{n}_{iK}^w$ accounts for the estimation error of the weighting coefficient caused by the correlated noise.

Equation (2) and Eq. (3) indicate the existence of a time delay τ_i between the signals of different antenna array elements. This delay results in a phase offset $\omega_{IF}\tau_i$ among the carrier phases. The phase weight compensates for this offset such that the signal carrier phases of each array element are aligned. Therefore, weight can be expressed as follows:

$$\hat{w}_i = e^{j\omega_{IF}\tau_i} = e^{-j\Delta\theta_i} = e^{-j(\theta_i-\theta_L)}, \tag{6}$$

where θ_i represents the carrier phase of antenna i, and θ_L represents the local carrier phase and is the common phase of the carrier after the phase alignment is completed. $\Delta\theta_i = \theta_i - \theta_L$ represents the phase offset between the antenna signal and local carrier.

All antennas underwent correlation weighting, and the antenna signals were coherently combined using a combiner. The combined signal of the antenna array can be expressed as follows:

$$\hat{C}_K = \sum_{i=0}^{L-1} \hat{S}_{iK} \hat{W}_{iK}^*, \tag{7}$$

where $\hat{C}_K$ is the combined output signal, L represents the number of elements of the antenna array, $\hat{S}_{iK}$ represents the satellite navigation signal with N sampling intervals as the time unit, the subscript K represents the signal at intervals of the K-th unit, $(\cdot)^*$ represents the complex conjugate of a complex signal.

As illustrated in Fig. 2 and proposed by Rogstad [19], the weight of the $K+1$-th unit, denoted as $\hat{W}_{iK+1}$, is updated and recursively obtained from the weight of the previous step $\hat{W}_{iK}$. The weight is calculated by correlating the reference signal $\hat{S}_{iK}^{Re}$ with $\hat{S}_{ik}\hat{W}_{iK}^*$ over a length of N, as follows:

$$\hat{W}_{iK+1} = \hat{W}_{iK} \left\{ \frac{1}{N} \sum_{k=KN}^{(K+1)N-1} \left[\hat{S}_{ik} \hat{W}_{iK}^* \hat{S}_{iK}^{Re} \right] \right\}, \tag{8}$$

$$\hat{S}_{iK}^{Re} = \hat{C}_k - \hat{S}_{ik}\hat{W}_{iK}^* + \hat{S}_k^L, \tag{9}$$

where $\hat{S}_{ik}$ represents the satellite navigation signal with the signal-sampling interval as the unit interval. The satellite navigation signal is an IF signal output by the RFFE, in which parameters such as carrier phase and carrier frequency are unknown, and are subsequently estimated by the PLL loop. $\hat{S}_k^L$ represents the local carrier signal.

Equation (7) shows that $\hat{S}_i$, L, and $\hat{W}_{iK}$ influence the combined signal. Equation (8) indicates that $\hat{W}_{iK}$ is related to N and $\hat{S}_{iK}^{Re}$. Thus, an analysis of the relationships between $\hat{C}_K$, $\hat{S}_{ik}$, L, and N is necessary.

4. Performance Analysis of Multi-Antenna Signal Combining

These principles reveal that the antenna signal CNR, number of antennas, and correlation time interval affect the combined-signal gain. The following presents a theoretical analysis of the CNR and carrier phase of the combined signal of the CPC algorithm compared with those of the conventional algorithm.

4.1 Analysis of the Combined-Signal CNR

The CPC algorithm primarily estimates the phase offset among the signals from various antennas in a distributed antenna array system owing to the difference in the transmission path. Compensating the offset through phase weights ensures phase alignment between all antenna signals, improving the correlation between the antenna signals and coherent additions to enhance the CNR of the combined signal. Because the capability of the algorithm to improve the CNR of the combined signal is a crucial evaluation index, this subsection presents an analysis focusing on the CNR of the combined signal.

To analyze the CNR of the combined signal, if no error is observed in the weight estimation of the signal combination, the optimal combination performance can be achieved. Equation (7) can be expressed as follows:

$$\hat{C}_K = \sum_{i=0}^{L-1} \left[\hat{s}_{iK} e^{-j\Delta\theta_i} + \hat{n}_{iK}^s e^{-j\Delta\theta_i} \right]. \tag{10}$$

In practice, the weight inevitably contains errors owing to the influence of noise, reducing the output CNR of the combined signal. Assumptions: (1) Each antenna has the same caliber and performance, (2) the received signal power remains stable, (3) Each antenna signal is aligned (affected by noise; the weights may not be optimal) and (4) the weights of each antenna signal are mutually uncorrelated. From Eq. (5), Eq. (10) can be divided into its signal and noise components. The average of the combined-signal power is P_{CS}, expressed as follows:

$$\begin{aligned} P_{CS} &= E\left| \sum_{i=0}^{L-1} \left[\hat{s}_{iK} e^{-j\Delta\theta_i} + \hat{s}_{iK} \hat{n}_{iK}^{w\,*} \right] \right|^2 \\ &= L^2 \left|\hat{s}_0\right|^2 + L \left|\hat{s}_0\right|^2 \left|\hat{n}^w\right|^2, \end{aligned} \tag{11}$$

where $\left|\hat{s}_0\right|^2$ and $\left|\hat{n}^w\right|^2$ represent the average power of the antenna signal and weight noise components, respectively. According to assumptions (1) and (2), the average power of the K-th unit can be replaced by the first moment of the K-th unit, $\hat{s}_{iK} = \hat{s}_0$. The average power of the combined noise component P_{CN} is expressed as

$$\begin{aligned} P_{CN} &= E\left| \sum_{i=0}^{L-1} \left[\hat{n}_{iK}^s e^{-j\Delta\theta_i} + \hat{n}_{iK}^s \hat{n}_{iK}^{w\,*} \right] \right|^2 \\ &= L \left|\hat{n}_0^s\right|^2 + L \left|\hat{n}_0^s\right|^2 \left|\hat{n}^w\right|^2, \end{aligned} \tag{12}$$

where $\left|\hat{n}_0^s\right|^2$ is the average power of the noise component of the antenna signal, $\hat{n}_{iK}^s = \hat{n}_0^s$. Therefore, the SNR of the combined signal can be expressed as follows:

$$\rho_c = \frac{P_{CS}}{P_{CN}} = \frac{L^2 \left|\hat{s}_0\right|^2 + L \left|\hat{s}_0\right|^2 \left|\hat{n}^w\right|^2}{L \left|\hat{n}_0^s\right|^2 + L \left|\hat{n}_0^s\right|^2 \left|\hat{n}^w\right|^2}. \tag{13}$$

Equation (13) can be simplified as follows:

$$\rho_c = \frac{L\rho_s + \rho_s \left|\hat{n}^w\right|^2}{1 + \left|\hat{n}^w\right|^2}, \tag{14}$$

where $\rho_s = \left|\hat{s}_0\right|^2 / \left|\hat{n}_0^s\right|^2$ represents the antenna signal SNR. The optimal performance of the algorithm is analyzed assuming that the antenna array has already undergone phase alignment. Under ideal conditions, represented by $\left|\hat{n}^w\right|^2 \to 0$, when the phase weight completely compensates for the phase offset, and the IF signals are optimally combined, the

combined-signal SNR can essentially achieve the theoretical performance, $\rho_c = L\rho_s$. However, the combined performance cannot reach the theoretical gain owing to the influence of weight noise. Therefore, the SNR loss factor caused by weight estimation errors can be defined as follows:

$$\gamma_\rho = \frac{1 + 1/L\,|\hat{n}^w|^2}{1 + |\hat{n}^w|^2}. \tag{15}$$

Rogstad [19] proposed the concept of weight $\hat{W}_{iK}$ and derived the SNR formula. The weight SNR is used to better analyze the phase-offset estimation error caused by noise in the algorithm. Therefore, in this study, the weight SNR ρ_w of the CPC algorithm is obtained as follows:

$$\rho_w \approx \frac{N\rho_s\rho_s - (1+\rho_s)\,L\mu}{\rho_s + (1+\rho_s)\,L\mu}, \tag{16}$$

where $\mu = R^2\,|\hat{s}_0|^4 \approx \left(\frac{1}{L}\right)^2$, where R is the normalization coefficient to prevent the phase weight amplitude from becoming unstable due to continuous accumulation. In the SUMPLE algorithm, the reference signal in each signal correlation operation is a combination of $L-1$ antenna signals. In the CPC algorithm, the reference signal also includes the local carrier signal. The local carrier signal is generated by the PLL and fed back to the signal synthesis algorithm. Therefore, the carrier signal frequency is equal to the antenna signal, but the phase is different from each antenna signal. That is, the local carrier signal and the antenna signal contain a same-frequency sinusoidal signal. Thus, in Eq. (16), the formula uses L rather than $L-1$. Unlike the SUMPLE algorithm aligns the antenna signal phases to an uncertain common phase, the CPC algorithm aligns the carrier phases of all antenna signals with the local carrier phases, thereby aligning the signal phases of each array element.

Figure 4 illustrates the relationship between ρ_s and ρ_c for various values of N. In this figure, $L = 6$, and the theoretical CNR increases by approximately 7.8 dB. Comparing the combined-signal curve for $N = 30$ ms with the antenna signal curve at a higher antenna signal CNR, the two curves were nearly parallel, indicating that the enhancement in the combined-signal CNR approached its limiting value. From Eq. (16), ρ_w decreased with the antenna signal CNR decreased. This decrease indicated the reduced credibility of the weights for the signal carrier phase and less ideal phase alignment effects. Resulting in the enhancement in the combined-signal CNR decreased as the antenna signal CNR. Notably, at an antenna signal CNR of 30 dB-Hz and $N = 20$ ms, the combined-signal CNR was lower than the antenna signal CNR. This phenomenon occurred because ρ_w became negative, indicating algorithm failure. In such cases, the signal carrier phases cannot converge, leading to significant losses in the combined-signal CNR. Comparing the three combined-signal curves, a smaller N led to a reduced combined-signal CNR. Therefore, the CNR of the combined signal was proportional to N.

Figure 5 illustrates the relationship between ρ_s and ρ_c

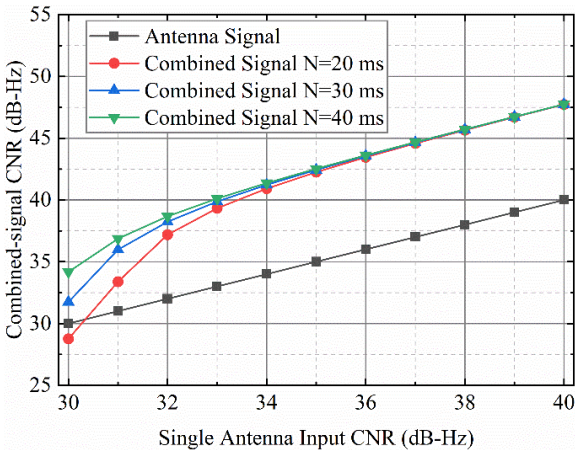

Fig. 4 Combining CNR for various correlation averaging intervals.

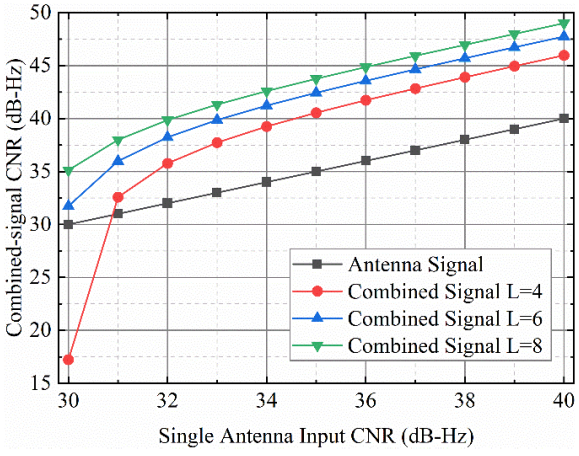

Fig. 5 Combining CNR for different numbers of antennas.

for different L, where $N = 30$ ms. The figure shows that an increase in L resulted in the enhancement of combined-signal CNR. The combined-signal CNR was directly proportional to L, consistent with the relationship expressed in Eq. (13). Similarly, the combination process incurred minimal losses at a higher antenna signal CNR, and the limit of the combined gain could be reached. At an antenna signal CNR of 30 dB-Hz and $L = 4$, the algorithm failed, resulting in a combined-signal CNR lower than the antenna signal CNR.

A simulation validation was conducted to assess the CNR enhancement performance of the CPC algorithm. The simulated signal was based on the GPS L1 C/A signal and characterized by the parameters presented in Table 1. Figure 6 compares the combined-signal CNR achieved by the CPC algorithm with that achieved by the conventional method. The CNR for the conventional algorithm was approximately 37.25 dB-Hz, whereas that for the CPC algorithm was approximately 38.20 dB-Hz. Compared with the single antenna signal CNR, the CPC algorithm has improved by 6.2 dB. Compared with the theoretical value, the combined CNR of the SUMPLE algorithm loses 2.52 dB,

Table 1 Simulation parameters.

Parameter	Value
Sampling frequency	24.552 MHz
Intermediate frequency	4.092 MHz
Noise bandwidth	2.046 MHz
CNR	32 dB-Hz
N	30 ms
L	6
Number of iterations	20

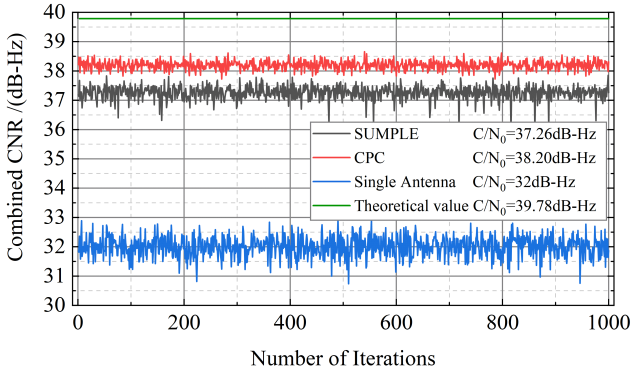

Fig. 6 Combined CNR for different algorithms.

the loss of the CPC algorithm is 1.58 dB, and the combined CNR is close to the theoretical value. Compared with the SUMPLE algorithm, the CNR loss of the CPC algorithm is reduced by about 1 dB. The combined-signal CNR was more stable because the reference signal $\hat{S}_{iK}^{Re}$ in the CPC algorithm contains the local carrier signal, which has high CNR and stable phase characteristics and enhances ρ_w. A higher ρ_w increased the combined-signal CNR and resulted in accurate phase-compensation values. Therefore, the phase alignment of the antenna array signals became stable, improving the stability of the CNR in the CPC algorithm.

4.2 Analysis of the Combined-Signal Carrier Phase

Equation (7) shows that the phase of the combined signal $\hat{C}_k$ is a function of time k. The phase is influenced by changes in $\hat{S}_{ik}$ and $\hat{W}_{iK}$. Assuming that the weight remains constant during the correlation time, the combined signal is integrated as

$$\begin{aligned}\hat{C}_{K+1} &= \frac{1}{ncor}\sum_{k=(K+1)N}^{(K+2)N-1}\left(\sum_{i=0}^{L-1}\hat{S}_{ik}\hat{W}_{iK+1}{}^{*}\right)\\ &= \hat{c}_{K+1}+\hat{n}_{K+1}^{c},\end{aligned} \tag{17}$$

where $\hat{c}_{K+1}$ and $\hat{n}_{K+1}^{c}$ correspond to the signal and noise components of the combined signal in $K+1$-*th* unit, respectively. The former is expressed as follows:

$$\hat{c}_{K+1} = \sum_{i=0}^{L-1}\left(\hat{s}_{iK}\hat{W}_{iK+1}^{*}\right). \tag{18}$$

Substituting Eq. (8) into Eq. (18) and simplifying it yields the following expression:

$$\begin{aligned}\hat{c}_{K+1} &= \left|\hat{W}_{iK}\right|^2|\hat{s}_0|^2\hat{c}_K+\left|\hat{W}_{iK}\right|^2|\hat{s}_0|^2\hat{S}_K^L(L-1)\\ &\quad+\sum_{i=0}^{L-1}\hat{s}_{iK}\hat{n}_{iK+1}^{w}{}^{*}.\end{aligned} \tag{19}$$

Equation (19) shows that $\sum_{i=0}^{L-1}\hat{s}_{iK}\hat{n}_{iK+1}^{w}{}^{*}$ and $\hat{S}_K^L$ influence the phase center of the combined signal. When using the conventional algorithm, during each signal correlation process, the reference signal is the weighted sum of all other antenna signals whose phase center is not fixed but varies owing to the influence of weight noise, causing the phase center of the combined signal to vary with time. Moreover, when the initial phase of each antenna signal is dispersed, the phase center may gradually deviate toward 0 or pi during the iteration process. This phenomenon can lead to convergence failure of conventional algorithms.

Rogstad [19] derived the combined-signal phase-compensation formula for the algorithm convergence problem as follows: $\Delta\hat{W}_{iK}=\sum_{i=0}^{L-1}\left(\hat{W}_{iK}\hat{w}_{iK-1}^{*}\right)$. However, $\hat{w}_{iK-1}$ in the equation is unknown; therefore, $\hat{W}_{iK}$ is used rather than $\hat{w}_{iK-1}$. This method is feasible when the SNR of the input signal is high because the weight noise $\hat{n}_{iK}^{w}$ is small, and $\hat{W}_{iK}$ can be approximately equal to $\hat{w}_{iK-1}$. However, in general, the existence of estimation errors adversely affects the compensation performance, causing the method to fail. By contrast, in the CPC algorithm, the phase of the local carrier signal remains constant and is added to the reference signal as a fixed-phase component. During each iteration, the phase of the antenna signals approaches this fixed component and eventually converges. This phenomenon effectively resolves the convergence problem in conventional algorithms.

Figure 7 compares the phase offset and correction versus iteration of the combined output for various algorithms, where the simulated signal is based on the GPS L1 C/A signal and characterized by the parameters presented in Table 1. The red line represents the phase of the combined signal using the SUMPLE algorithm, whereas the blue line represents the phase of the combined signal after using the SUMPLE algorithm and correcting the phase. The comparison revealed that although phase compensation reduced the combined phase error, it did not yield a significant improvement. The black line represents the phase of the combined signal using the CPC algorithm, showing a noticeable reduction in the phase error compared with the other two cases, with errors within 5°. Compared with that of the SUMPLE algorithm after phase compensation, the phase error variance of the CPC algorithm was reduced by 80%, and the stability was significantly improved.

Figure 8 shows the convergence performance of different algorithms, where the signal parameters are as shown in Table 1. From the figure, within 20 iterations of the CPC algorithm, the CNR of the combined output signal tends to be stable, and the algorithm completes convergence. The

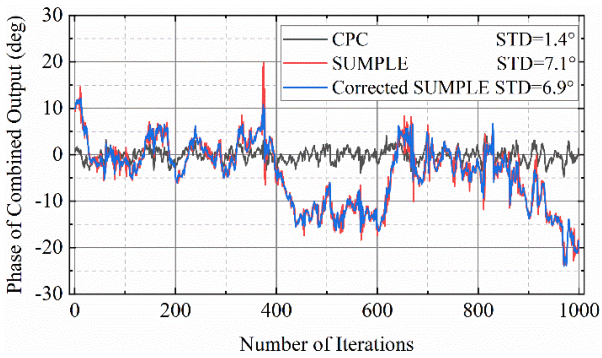

Fig. 7 Phase offset and correction versus iteration of the combined output for various algorithms.

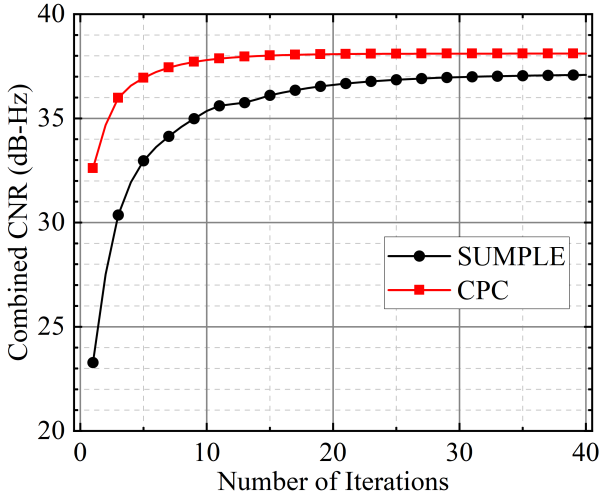

Fig. 8 Convergence performance for various algorithms.

SUMPLE algorithm converges within approximately 30 iterations. Moreover, the CNR of the combined signal of the CPC algorithm is higher than that of the SUMPLE algorithm, which is consistent with the results in Fig. 6.

5. Simulation Result and Performance Analysis

Simulation experiments were performed to validate the efficacy of the CPC algorithm in terms of the signal gain and phase alignment. The simulated signal was based on the GPS L1 C/A signal and characterized by the parameters presented in Table 1. In the experiment, the CNR of the navigation signal changed in the static environment of the receiver.

Figure 9 compares the theoretical combined-signal CNR deduced using Eq. (13) with the simulated combined-signal CNR. The simulated signal was enhanced by nearly 7 dB compared with the single-antenna signal when $\rho_s >$ 33 dB-Hz, consistent with the theoretical prediction. Comparing the theoretical and simulated curves, these results were consistent when $\rho_s >$ 33 dB-Hz. Below 33 dB-Hz, the simulated signal curve deviated from the theoretical curve, progressively increasing the discrepancy. This is because the antenna signal CNR decreases, the weight noise gradually increases, and the phase weight becomes more difficult to achieve the assumption of the optimal weight. The simulated signal CNR value was 1.6 dB lower than the theoretical value when ρ_s = 30 dB-Hz, which was improved by approximately 2.5 dB compared with the CNR value of a single antenna.

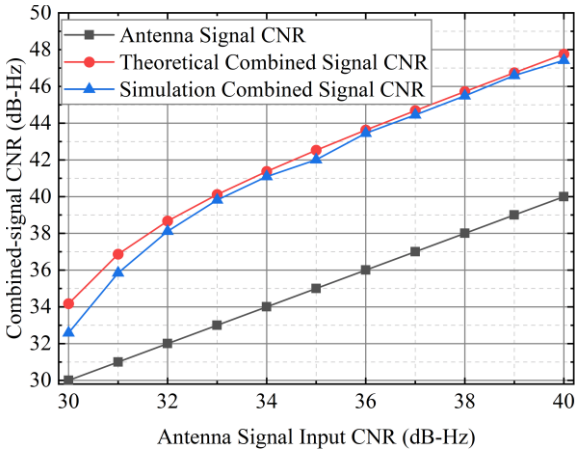

Fig. 9 Difference of combining CNR between simulation and theory.

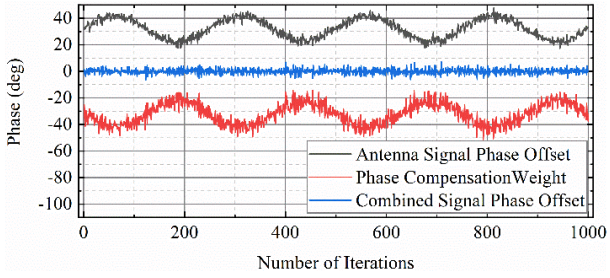

Fig. 10 CPC phase wander and correction versus iteration.

Figure 10 shows the simulation verification of the phase convergence of the CPC algorithm, in which a phase shift is added to the antenna signal carrier phase. The black curve represents the phase offset between the antenna and local carrier signals. The red curve represents the phase-compensation values applied by the CPC algorithm to the antenna signals. The compensatory phase exhibited an inverse relationship with the black curve, indicating that the CPC algorithm could effectively perform phase compensation on the antenna signal to align it with the local carrier signal. The blue curve represents the phase offset between the combined and local carrier signals after the phase alignment using the CPC algorithm and the blue curve value is within 5°, consistent with Fig. 7.

As shown in Fig. 11, six GPS baseband signals at different locations were simultaneously generated through GPS-SDR-SIM software to simulate the distributed antenna array receiving signals. The signal parameters were consistent with those listed in Table 1. The blue curve represents changes in the antenna signal CNR. The initial CNR of all antenna signals was 40 dB-Hz, which gradually decreased to 30 dB-Hz and reverted to 40 dB-Hz. Each signal

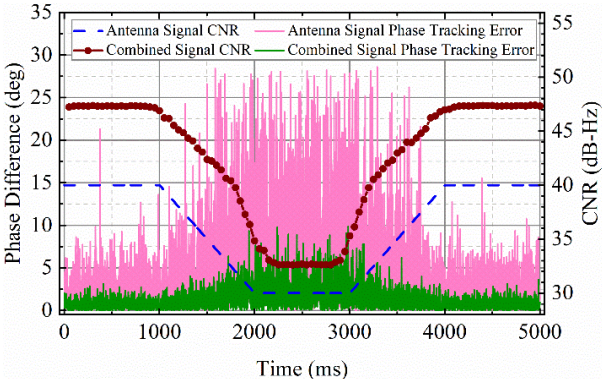

Fig. 11 Tracking performance between single and combined signals for various antenna signal CNRs.

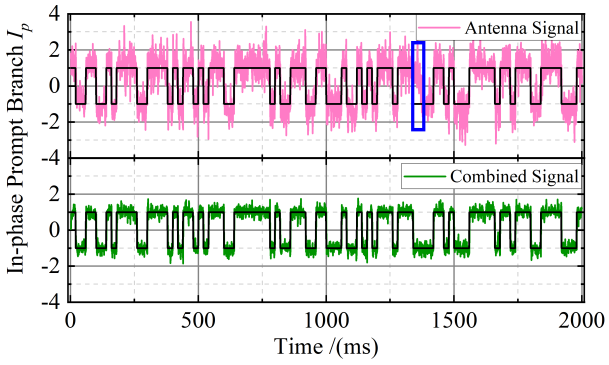

Fig. 12 PLL correlator output value I_p (navigation message).

segment persisted for 1000 ms. The brown curve represents the CNR of the combined signal calculated using the narrowband and wideband power ratios. When the antenna signal CNR was 40 dB-Hz, an enhancement of approximately 7.5 dB was observed, close to the theoretical value. When the CNR dropped below 33 dB-Hz, the enhancement value of the combined-signal CNR rapidly diminished, consistent with Fig. 9.

After 1000 ms, the CNR of the antenna signal decreased. At this point, the absolute value of the phase-tracking error in the PLL of the antenna signal increased rapidly. When the CNR decreased below 35 dB-Hz, the phase-tracking error was approximately 27°, indicating that the tracking loop was essentially out of lock. Compared with the antenna signal, the combined signal had more minor phase-tracking errors, and the performance improvement was more evident at a low CNR. When the antenna signal CNR was 30 dB-Hz, the phase-tracking error of the combined signal was maintained within 10°, and the phase variance was 2.3. By contrast, the phase variance of the antenna signal was 8.32, and the phase variance of the combined signal was approximately 72% lower than that of the antenna signal.

Figure 12 shows the in-phase prompt correlation values of the correlator output for antenna signal and combined signal carrier tracking loop. GPS navigation message information is obtained by binarizing the I_p value into 1 and −1 and demodulating it into a data bit stream. Therefore, the accuracy of the demodulation of the correlated value I_p affects the accuracy of the positioning result [35]. From the blue box in the picture, the decoding result of the antenna signal in-phase real-time correlation value I_p at 1340–1360 ms is wrong, which will lead to errors in subsequent positioning results. The decoding result of the combined signal in the figure is consistent with the real navigation message, and there is no decoding error.

6. Conclusion

This study investigated a multi-antenna signal-combining method in weak-signal environments. A CPC algorithm was proposed to effectively estimate phase offset and enhance signal gain. Theoretical derivation and analysis of the CPC algorithm demonstrated the relationship of the phase weight to the CNR of the combined signal. A higher CNR of the antenna signal, longer correlation time, and more array antennas indicated a smaller weight noise and superior algorithm performance. The results of the analysis and verification using a simulation platform demonstrated that the experiment results were consistent with those of the theoretical analysis. When using a distributed antenna array with six elements, the CPC algorithm could enhance the combined-signal CNR by 6 dB at 32 dB-Hz, exhibiting a 1 dB improvement compared with that of the SUMPLE algorithm. Moreover, the CPC algorithm could effectively estimate the phase offset between the signals of each array element, and the carrier phase error of the combined signal was maintained within 5°. Furthermore, tracking the combined signal through a PLL revealed that the phase-tracking error remained within 10° at 30 dB-Hz, representing a reduction of approximately 72% in the error compared with the antenna signal.

Acknowledgments

This work was supported by the National Key Research and Development Program of China under Grant 2021YFB3900703, and the National Science Foundation of China under Grant 41974038.

References

[1] E.D. Kaplan and C. Hegarty, eds., Understanding GPS: Principles and Applications, 2nd ed., Artech House, Boston, 2006.
[2] F.S.T.V. Diggelen, A-GPS: Assisted GPS, GNSS, and SBAS, Artech House, 2009.
[3] M.K. Bek, E.M. Shaheen, and S.A. Elgamel, "Analysis of the global position system acquisition process in the presence of interference," IET Radar, Sonar & Navigation, vol.10, no.5, pp.850–861, June 2016.
[4] H. Qin, X. Xue, and Q. Yang, "GNSS multipath estimation and mitigation based on particle filter," IET Radar, Sonar & Navigation, vol.13, no.9, pp.1588–1596, Sept. 2019.
[5] G. Gao, "INS-assisted high sensitivity GPS receivers for degraded signal navigation," vol.68, no.04, Library and Archives Canada = Bibliothèque et Archives Canada, Ottawa, 2007.
[6] P. Fan, X. Cui, S. Zhao, G. Liu, and M. Lu, "A two-step stochastic

hybrid estimation for GNSS carrier phase tracking in urban environments," IEEE Trans. Instrum. Meas., vol.70, pp.1–18, 2021.
[7] F. Xie, J. Liu, R. Li, and Y. Hang, "Adaptive robust ultra-tightly coupled global navigation satellite system/inertial navigation system based on global positioning system/BeiDou vector tracking loops," IET Radar, Sonar & Navigation, vol.8, no.7, pp.815–827, Aug. 2014.
[8] P.O. Gaggero and D. Borio, "Ultra-stable Oscillators: Limits of GNSS coherent integration," Proc. 21st International Technical Meeting of the Satellite Division of The Institute of Navigation (ION GNSS 2008), pp.565–575, Sept. 2008.
[9] X. Zhang, B. Guo, F. Guo, and C. Du, "Influence of clock jump on the velocity and acceleration estimation with a single GPS receiver based on carrier-phase-derived Doppler," GPS Solut, vol.17, no.4, pp.549–559, Oct. 2013.
[10] X. Feng, T. Zhang, X. Niu, T. Pany, and J. Liu, "Improving GNSS carrier phase tracking using a long coherent integration architecture," GPS Solut, vol.27, no.1, p.37, Dec. 2022.
[11] J.B.-Y. Tsui, Fundamentals of Global Positioning System Receivers: A Software Approach, John Wiley & Sons, Hoboken, NJ, USA, 2005.
[12] R.V. Kurynin, "A method of evaluating the g-sensitivity of quartz oscillators in GNSS receivers," 2019 Systems of Signal Synchronization, Generating and Processing in Telecommunications (SYNCHROINFO), Russia, pp.1–5, July 2019.
[13] D.H. Rogstad, A. Mileant, and T.T. Pham, Antenna Arraying Techniques in the Deep Space Network, John Wiley & Sons, 2005.
[14] S. Blandino, F. Kaltenberger, and M. Feilen, "Wireless channel simulator testbed for airborne receivers," 2015 IEEE Globecom Workshops (GC Wkshps), San Diego, CA, USA, pp.1–6, Dec. 2015.
[15] J. Huang, Y. Su, W. Liu, and F. Wang, "Adaptive modulation and coding techniques for global navigation satellite system inter-satellite communication based on the channel condition," IET Communications, vol.10, no.16, pp.2091–2095, Nov. 2016.
[16] M. Sadeghi, F. Behnia, and R. Amiri, "Maritime target localization from bistatic range measurements in space-based passive radar," IEEE Trans. Instrum. Meas., vol.70, pp.1–8, 2021.
[17] M. Rashid and J.A. Nanzer, "Frequency and phase synchronization in distributed antenna arrays based on consensus averaging and Kalman filtering," IEEE Trans. Wireless Commun., vol.22, no.4, pp.2789–2803, April 2023.
[18] D. Divsalar, "Symbol stream combining versus baseband combining for telemetry arraying," The Telecommun. and Data Acquisition Rept., pp.13–28, Aug. 1983.
[19] D.H. Rogstad, "The SUMPLE algorithm for aligning arrays of receiving radio antennas: Coherence achieved with less hardware and lower combining loss," Interplanetary Network Progress Report, vol.42–162, pp.1–29, Aug. 2005.
[20] K.-M. Cheung, "Eigen theory for optimal signal combining: A unified approach," Telecommunications and Data Acquisition Progress Report, vol.126, pp.1–9, April 1996.
[21] V.A. Vilnrotter and E.R. Rodemich, "A real-time signal combining system for Ka-band feed arrays using maximum-likelihood weight estimates," The Telecommunications and Data Acquisition Report, Feb. 1990.
[22] J. Xu, S. Ni, and Y. Yang, "Analysis of distributed synthesis algorithm based on simple and sumple algorithm," 2021 IEEE 4th Advanced Information Management, Communicates, Electronic and Automation Control Conference (IMCEC), Chongqing, China, pp.1327–1332, June 2021.
[23] C. Chen, H. Yu, C. Shen, C. Tan, A. Zhang, and Z. Tang, "A combining algorithm for signal arraying using MMSE estimator," 2009 Fourth International Conference on Communications and Networking in China, Xian, China, pp.1–4, Aug. 2009.
[24] L. Wang and D. Wang, "A gain factor controlled SUMPLE algorithm and system," 2017 IEEE 12th International Conference on ASIC (ASICON), Guiyang, pp.183–186, Oct. 2017.
[25] Y. Di, S. Weiyi, L. Peijie, S. Ke, and L. Xiaoyu, "Parallel implementation of SUMPLE algorithm in large-scale antenna array," Communications, Signal Processing, and Systems, Singapore, pp.433–439, 2020.
[26] S. Ni and J. Xu, "A distributed receiving synthesis algorithm based on resampling," Telecommunication Engineering, vol.63, no.5, pp.676–680, 2023.
[27] P. Siu, C. Apker, J. McMillen, and S. Sorber, "G-STAR GPS anti-jam technology," Proc. 2006 National Technical Meeting of The Institute of Navigation, pp.1057–1063, Jan. 2006.
[28] D. Rowe, J. Weger, and J. Walker, "Integrated GPS anti-jam systems," Proc. 18th International Technical Meeting of the Satellite Division of The Institute of Navigation (ION GNSS 2005), pp.1–7, Sept. 2005.
[29] S. Backen, D.M. Akos, and M.L. Nordenvaad, "Post-processing dynamic GNSS antenna array calibration and deterministic beamforming," Proc. 21st International Technical Meeting of the Satellite Division of The Institute of Navigation (ION GNSS 2008), pp.2806–2814, Sept. 2008.
[30] N. Vukmirović, M. Erić, M. Janjić, and P.M. Djurić, "Direct wideband coherent localization by distributed antenna arrays," Sensors, vol.19, no.20, p.4582, Oct. 2019.
[31] X. LI, P. LI, X. Liu, and Z. He "Signal combination of distributed antenna array using power inversion criteria," Telecommunication Engineering, vol.60, no.12, p.1432, 2020.
[32] R.T. Compton, "The power-inversion adaptive array: Concept and performance," IEEE Trans. Aerosp. Electron. Syst., vol.AES-15, no.6, pp.803–814, Nov. 1979.
[33] L. Lu and M. Gao, "A satellite calibration method for the baseline coordinate and phase difference of distributed radar array," Journal of Electronics & Information Technology, vol.41, no.12, pp.2896–2902, 2019, doi: 10.11999/JEIT181152.
[34] H. Tong, "Joint processing for satellite navigation signals," Ph.D, National University of Defense Technology, 2014.
[35] K. Borre, D.M. Akos, N. Bertelsen, P. Rinder, and S.H. Jensen, A Software-Defined GPS and Galileo Receiver, Birkhäuser, Boston, MA, 2007.

Wenfei Guo is currently a professor in GNSS Research Center, Wuhan University (WHU). He received his PhD degree in communication and information system from Wuhan University, Wuhan, China, in 2011. His research interests include GNSS receivers and related signal processing technologies, including high-precision timing receivers, anti-jamming receivers, and LEO navigation, etc.

Jun Zhang was born in 1999. He received the B.E. degree in electronic information school from Wuhan University, Wuhan, China, in 2017. He is currently pursuing the M.S. degree with the GNSS Center, Wuhan University, Wuhan, China. His current research interests include GNSS baseband signal processing, GPS acquisition and tracking algorithm.

Chi Guo received the Ph.D. degree in computer science from Wuhan University, Wuhan, Hubei, China, in 2010. He is currently a professor with the National Satellite Positioning System Engineering Technology Research Center, Wuhan University. His current research interests include BeiDou application, unmanned system navigation, and location-based services (LBS).

Weijun Feng was born in 2000. He received the B.E. degree in communication engineer school from Hangzhou Dianzi University, Hangzhou, China, in 2018. He is currently pursuing the M.S. degree with the GNSS Center, Wuhan University, Wuhan, China. His current research interests include Iridium satellite signal baseband signal processing and position method.